Testing Procedure for the Single Fiber Fragmentation Test

Feih, Stefanie; Wonsyld, Karen; Minzari, Daniel; Westermann, Peter; Lilholt, Hans

Publication date:
2004

Document Version
Publisher's PDF, also known as Version of record

RISØ

Risø-R-1483(EN)

Testing procedure for the single fiber fragmentation test

Stefanie Feih, Karen Wonsyld, Daniel Minzari, Peter Westermann, and Hans Lilholt

Risø National Laboratory
Roskilde
Denmark
December 2004

Author: Stefanie Feih, Karen Wonsyld, Daniel Minzari, Peter Westermann, Hans Lilholt
Title: Establishing a Testing Procedure for the Single Fiber Fragmentation Test
Department: AFM, Department for Material Research

Abstract (max. 2000 char.):

This report describes the details of the single fiber fragmentation test as conducted at the materials research department (AFM) at Risø. The equipment and specimen manufacture is described in detail. Furthermore, examples of results interpretation are given.

For the experiments in this report, specimens with one E-glass fiber placed inside an epoxy or polyester matrix were used. Elongating the specimens with a mini tensile tester, which was placed under a microscope, leads to fiber fragmentations. Different bonding strengths between fiber and matrix result in differences in the critical fracture length for the fiber and fracture characteristics.

Print: Pitney Bowes Management Services Denmark A/S, 2004

Risø-R-1483(EN)
December 2004

ISBN 87-550-3381-4(Internet)
ISSN 0106-2840

Contract no.:

Groups own reg. no.:
1615070-00

Sponsorship:

Cover:

Pages: 30
Tables: 2
Figures: 23
References: 16

Risø National Laboratory
Information Service Department
P.O.Box 49
DK-4000 Roskilde
Denmark
Telephone +45 46774004
bibl@risoe.dk
Fax +45 46774013
www.risoe.dk

Contents

1 Introduction

One of the primary objectives in the field of fiber-polymer composites is the control of the degree of adhesion between the usually more rigid fiber and the relatively ductile polymer matrix. Interface tailoring involves challenging scientific and technological problems, and the complex issue of interface design directly influences the macroscopic composite properties.

A major problem is the development, analysis and better understanding of micromechanical methods designed to provide a quantitative measurement of the adhesion between a fiber and the surrounding polymer matrix. Round robin tests involving a variety of test methods (e.g., single-fiber fragmentation test, microbond test, single fiber pull-out test, single fiber compression test) [1] have shown that different tests are unable to provide similar answers for the level of interface adhesion of a given composite system. Even for the same test, round robin exercises [2] show that different results are obtained in different laboratories. However, although these tests up to now do not result in quantitative measures for the adhesion between fiber and matrix, a given test procedure at a given laboratory can be used to characterise and compare different composite systems.

At present, the single fiber fragmentation test (SFFT) is one of the most popular methods to evaluate the interface properties of fiber-matrix composites. The method has been used extensively [3-6] to determine the bonding characteristics between fiber and matrix on the microscale.

2 Background of the Fragmentation Test

The fragmentation test is developed from the early work of Kelly and Tyson [7], who investigated brittle tungsten fibers that broke into multiple segments in a copper matrix composite. Each test specimen for the fragmentation test consists of one fiber encapsulated in a chosen polymer matrix. The specimen normally has a dogbone shape. Elongating the specimens in a tensile tester results in fiber breakage. This experiment is done under a light microscope so that the fragmentation process can be observed in-situ. The fiber inside the resin breaks into increasingly smaller fragments at locations where the fiber's axial stress reaches its tensile strength. This requires a resin system with a sufficiently higher strain-to-failure than the fiber's. When the fiber breaks, the tensile stress at the fracture location reduces to zero. Due to the constant shear in the matrix, the tensile stress in the fiber increases roughly linearly from its ends to a plateau in longer fragments. The higher the axial strain, the more fractures will be caused in the fiber, but at some level the number of fragments will become constant as the fragment length is too short to transfer enough stresses into the fiber to cause further breakage. The process is sketched in Figure 1.

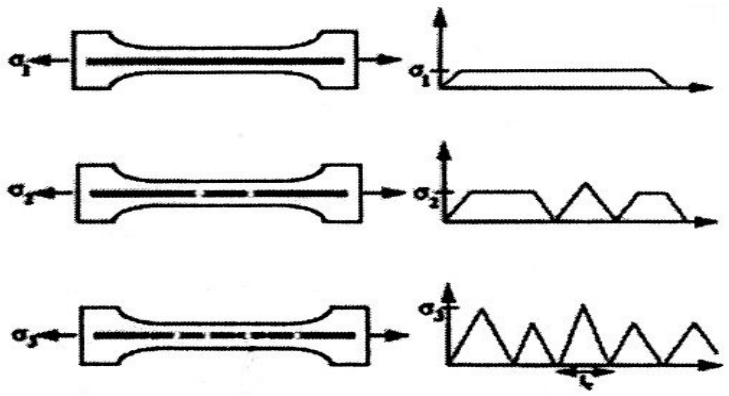

Figure 1: Left: Specimen with increasing number of fiber breaks due to increased strain levels in the matrix. Right: Stress in fiber as function of position for the respective matrix strain levels. Zero stress corresponds to a position with a fiber break [2].

The average shear strength at the interface, whether bonded, debonded or if the surrounding matrix material has yielded, whichever occurs first, can be estimated from a simple force balance equation for a constant interfacial shear stress [7]:

$$\tau = \frac{\sigma_f\left(l_c\right)\, d}{2l_c},$$

where σ_f is the fiber strength at the critical length, d is the fiber diameter and l_c is the critical fragment length of the fiber.

The critical fragment length was discussed in detail in [8]. Consider a single fiber embedded into a matrix material, when the test specimen is subsequently submitted

to axial tension. If the system is elongated, the stress transferable to the fiber at a distance x from the fiber end is given by:

$$\sigma_x = \frac{4\tau}{d} x$$

When the specimen is elongated further, the tensile stress of the fiber, σ_x, increases until it reaches the ultimate strength of the fiber, σ_f. If the value of x at this particular point is designed as x_0, the following relationship results:

$$\sigma_f = \frac{4\tau}{d} x_0 .$$

The fiber can break at any point along its length away from the fiber end by x_0. If a broken piece exceeds $2x_0$ in length, the breakage repeats itself by the same mechanism above. Once all the broken pieces are reduced to less than $2x_0$, any further elongation of such pieces does not cause the tensile stress transferable to the fiber, σ_x, to reach the ultimate tensile strength, σ_f. No further fragmentation takes place. The length of broken fiber pieces, l, should be distributed in the range $x_0 < l < 2x_0$, and the average value is given as follows

$$\bar{l} = \frac{1}{2}(x_0 + 2x_0) = \frac{3}{2} x_0 .$$

Since x_0 is the length needed to introduce the ultimate tensile strength, the critical fiber length is equal to $2x_0$. Introducing this into the relationship above leads to the following relationship for the critical fiber length:

$$l_c = \frac{4}{3} \bar{l} .$$

In order to determine the interfacial shear stress, one therefore measures the average fragment length at saturation stage (no more breaks occur when applying further strain to the specimen). From this, calculation of the critical length and interfacial shear strength can be done. A stronger bond between fiber and matrix results in a shorter critical fragment length.

Furthermore, the shape of the fiber breaks and the debonding characteristics between fiber and matrix are characteristic for the composite system. If the bonding at the interface is strong, the fiber cracks will propagate into the matrix and cause the matrix to deform around the crack. On the other hand, if the interface bonding is weak, debonding between fiber and matrix occurs and the fiber slips out. Both the breaking gap and the debonding zone will become wider with the matrix being entirely or almost entirely intact. In some cases, both events can occur. These aspects provide a wide range of information about the adhesion for one test specimen, which is the main advantage of the SFFT.

3 Specimen manufacture

3.1 Resin specimens without fiber (calibration)

The specimens were cut with an x-y-z machine from a 2 mm thick epoxy or polyester plate, respectively. The specimen shape can be seen in Figure 2. The angled tab shape fits the holder shape and prevents the specimen from sliding out during loading. No gripping of the specimen is required.

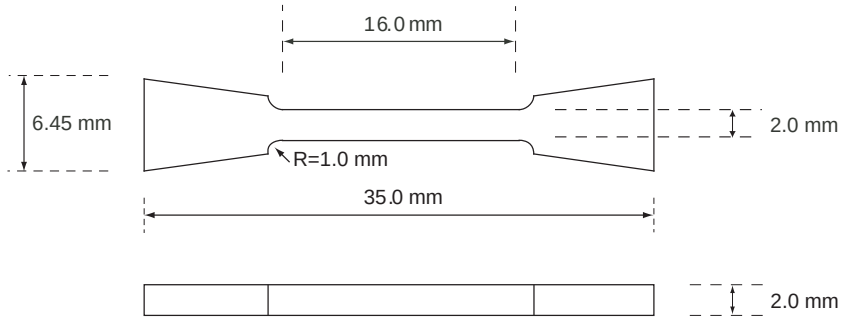

Figure 2: Specimen dogbone shape for fragmentation test

It should be noted that the form of the specimen is of course arbitrary and depends on type of holder in the testing equipment. The gauge length of the specimens should be long enough to get a high number of fiber fragments.

3.2 Resin specimens with fiber

1) A metallic negative of the specimens in Figure 2 is made on an x-y-z machine with slots at each end to be able to place the fiber in the middle of the resin specimen. The height of these metal slots is half the height of the specimen thickness to place the fiber in the middle of the specimen (see Figure 3 (a)).
2) Silastic 3120RTV Silicone Rubber and Dow Corning Catalyst (polysiloxane) is mixed in ratio 10:1 respectively and put into the steel mould. About 20 g for each form is used. The mould is cured over night at room temperature. Red silicone is chosen as the white glass fiber can be seen well against this background. (see Figure 3 (b)).


(a)

(b)

Figure 3: (a) Steel mould for production of silicon forms. (b) A silicon form for specimen fabrication.

3) At each end of the fiber a metal weight of 10g is attached with metal clamps. The metal clamps are lined with black rubber to soften the contact area with the fibers.
4) The form is placed on the pre-straining set-up, which is inside the oven to avoid having to move the specimens around, and the fiber with the weights is drawn over the rolls and placed in the form (see Figure 4). The central alignment needs to be controlled.

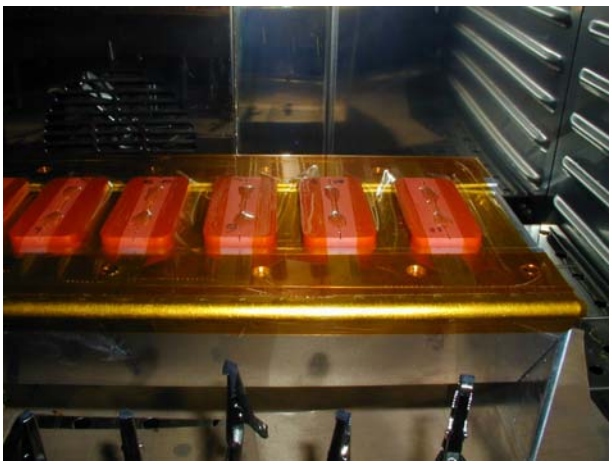

Figure 4: Pre-straining set-up. The weights are fixed onto the fiber with metallic clamps.

5) The specimen form is filled up with resin using a pipette. There has to be added as much resin in the form as possible (using the surface tension) because it shrinks when curing. For resins with high curing shrinkage it is necessary to refill the forms once it begins to gel.
6) The curing takes place according to the curing schedule.
7) The specimens are removed from the form and polished first with 1000 and then with 4000 paper until they are transparent, and the fiber can be clearly seen against the light. A typical specimen can be seen in Figure 5.

Figure 5: Polyester specimen.

3.3 Pre-straining the fiber

Pre-straining the fiber during the manufacture is of high importance. There are two reasons for this [5]: (1) The glass fiber has a high strain-to-failure, which is close to the yield strength of many polymeric matrix systems used in composites, and (2) thermal residual stresses due to resin curing introduce compressive strains in the fiber, and thus the fiber must elongate more in order to break under tension. Therefore, the saturation limit for fiber breakage can often only be reached if fiber

pre-straining compensates for the two arguments above. Specimens as manufactured in the previous section are only used for testing if the weights are still connected to the fiber at the end of the pre-curing cycle.

Weights of 10g lead to a pre-strain of about 0.65 % for a typical glass fiber with 16μm and Young's modulus of 76 GPa. For carbon fibers with an average of 8 μm diameter and Young's modulus of 320 GPa, a 10g weight results in 0.6 % strain. The similar value is due to the higher Young's modulus.

The far field fiber stress $\sigma_{f,\infty}$ includes the applied tensile stress, the (compressive) thermal stress and the imposed (tensile) pre-stress due to the weights. Thus, a one-dimensional analysis of the applied tensile stress leads to superposition of these strains and stresses:

$$\sigma_{f,\infty} = \sigma_m \frac{E_f}{E_m} + \sigma_f^{th} + \sigma_{pre} \qquad \text{or} \qquad \varepsilon_{f,\infty} = \varepsilon_m + \varepsilon_f^{th} + \varepsilon_{pre} \ ,$$

where $\sigma_{f,th}$ is negative and may be calculated from simple one-dimensional models:

$$\sigma_f^{th} = \left(\alpha_m - \alpha_f\right)\left(T - T_{ref}\right)\frac{E_f}{1+\left(\frac{\phi_f}{\phi_m}\right)\left(\frac{E_f}{E_m}\right)},$$

in which the factor ϕ_f/ϕ_m denotes the volume fractions of glass and resin. It is negligible for a single fiber within a cross-sectional area of 4mm^2. T is the room (or testing) temperature and T_{ref} the reference temperature of the specimen at which the fiber is stress-free. For E-glass, the thermal expansion coefficient is α_f=5.1x10^{-6} C^{-1}. The reference temperature is more difficult to determine. According to Detassis et al. [9], for epoxies with two curing temperatures this stress-free temperature is about the same as the post-curing temperature. This value is consequently chosen in related articles when calculating residual stresses. There is only one curing temperature for the polyester resin, which is chosen as the stress-free temperature.

Table 1 gives some typical values for the two resin systems.

	Epoxy	Polyester
Modulus [GPa]	2.8	3.4
Expansion coefficient, α_m [10^{-6} 1/K]	72.5[1]	~100[2]
Curing temperature (solidification) [°C]	40	50
Post-curing temperature [°C]	120	--
Stress-free temperature [°C]	120 [9]	50
Compressive strain at 20°C, $\varepsilon_{f,th}$ [%]	-0.7	-0.3
Pre-strain, ε_{pre} [%]	0.65	0.65
Strain of first fiber failure, ε_m (Exp. result) [%]	~2.0	~2.0

[1]as specified by manufacturer
[2]average value for polyester resins

Table 1: Strains in specimen after manufacture

It should be noted that the above calculations neglect the curing shrinkage. However, for epoxy it has been shown that the residual stresses due to cooling are much larger than the curing shrinkage stresses, which only contribute with 5% of the total residual stress [10]. They can therefore be neglected. For polyester, on the other hand, the total volume curing shrinkage is given as 8% (linear 2.33%) by the manufacturer, and shrinkage of the resin volume is indeed also observed during manufacture. However, most of this curing shrinkage takes place during the beginning of the solidification process. At this point more resin is added to the still liquid resin in the mould to compensate for this shrinkage and ensure the correct specimen thickness. As the fragmentation onset is about the same for epoxy and polyester specimens, the difference between the thermal compressive strain for the epoxy and polyester in the order of 0.4% can either be explained by additional resin shrinkage or a higher expansion coefficient α, which is currently assumed from literature values.

The average fiber strain to failure is 2±0.6% as established in earlier experiments [11], and the experimental starting value for fracture occurs at about 2% for fibers with strong interfacial bonding for both epoxy and polyester. This fits within the experimental uncertainties with the residual strain calculation.

4 Test equipment

4.1 Tensile tester

The main piece of the test equipment consists of a custom-made tensile testing equipment designed to pull both ends of the specimen slowly apart. This results in a uniform tensile stress distribution in the gauge section of the specimen. This apparatus is placed on top of an x-y-table and a holder is mounted on the back to connect the apparatus to the light microscope (see Figure 6).

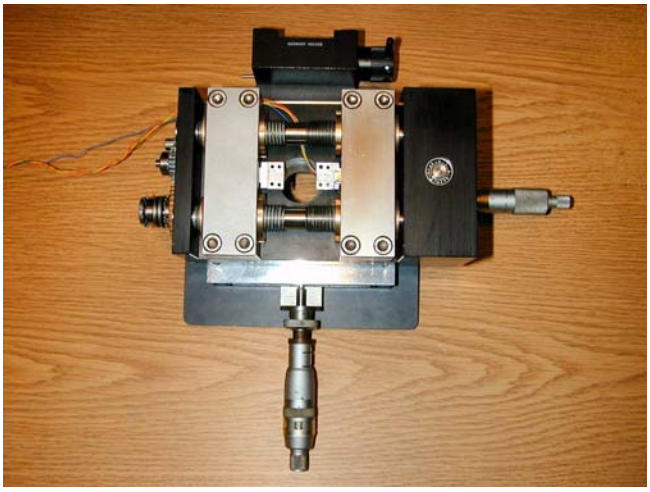

Figure 6: Test apparatus with specimen holders. The grey micrometer screws are used for moving the x-y-table and recording the fiber break positions inside the specimen. On top of the picture is a grip that holds the apparatus on the focusing mechanics of the microscope.

4.2 Fragmentation equipment

The whole set-up for the fragmentation tests consists of a light microscope, the tensile tester described in Section 4.1, a motor with wire for connection with the test apparatus, a strain measurement box, an electrical current box and a switch box with push and pull switch and speed regulator. The fragmentation set-up can be seen in Figure 7.

The equipment is connected as follows:

1) The x-y-table, which can be attached to the microscope, is fixed to the test apparatus. The x-y-table and the apparatus both have a hole under the specimen to allow the transmittant light source to be used during the test.
2) A flexible wire connecting the machine and the motor is fabricated. Inside is a fiber wire and on top of that are two layers of rubber, which are shrunken by heat so that they fit closely around the fibers and in the ends around the connection on the motor and the rotate handle on the machine.
3) The motor is placed so that the wire bends softly to be able to move the x-y-table during testing.
4) A full Wheatstone bridge (see also Section 4.4 and 4.5) is applied for strain measuring to one of the specimen holders. It is important to make sure that

the connections are not covering the part of the grip that goes into the machine.

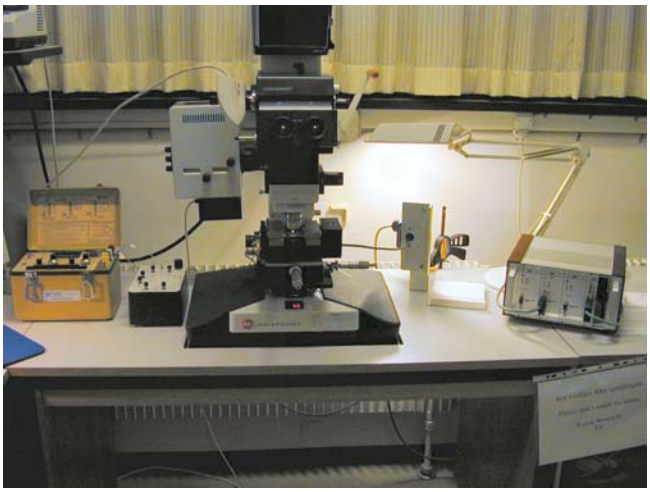

Figure 7: Test set-up. From left side: Strain measurement box, which is connected to one of the specimen holders, switch box with push and pull switch and speed regulator connected to the motor, microscope with test apparatus, motor connected with a wire to the tensile tester, electrical current box.

4.3 Fragmentation under microscope

1) The test apparatus is placed under a light microscope on top of a pair of springs. The apparatus weighs 8 kg and is too heavy for the microscope to lift when focussing without support. The stage is only designed for 4 kg and the equipment can damage the internal microscope mechanism without additional support. Rubber bands can also be used instead of the springs.
2) A motor and a left/right switch are connected to the apparatus with a wire.
3) The grey microscope screws for x-y movement are fixed to the x-y-table.
4) Specimen holders are placed in the apparatus and connected with a strain gauge box.

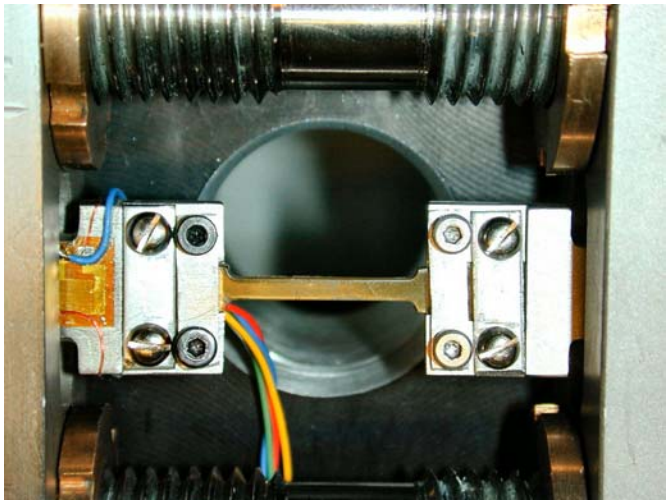

Figure 4.6: Specimen in the test apparatus.

5) When a specimen is placed in the apparatus, the specimen under the microscope can be moved in the x-direction with the micrometer screw. The optical lens with a magnification of 20 is normally used during the test to take enlarged pictures of the fragments. 1.6 can be used to study the whole specimen during the test to determine the fracture onset accurately. There is only room for one optical lens due to the dimensions of the tensile tester - the others need to be taken out of the optics holder.
6) Pulling the specimen. This is done slowly to avoid the specimen from breaking too early. The axial loading is continued until full fragmentation is reached or the resin breaks. The approximate specimen strain can be read from the box display of the Wheatstone bridge (see Section 4.4 and 4.5).
5) Strain measurement directly on the specimen can be used for improved accuracy (see Section 4.6).
7) Pictures of the breaks are taken and if full fragmentation occurs, the length of the fragments and of the breaks is measured.
6) Pictures can be taken with polarised light for additional information. To see the birefringence pattern, the cross-polarizers are used (see Section 4.7) – one above and one below the specimen (the one above is built into the microscope and only needs to be pushed in). The one below is a standard Nikon camera polarizer, which is placed on the light source below the specimen.

4.4 Force/strain measurement from box display (Wheatstone bridge)

The experiment is displacement controlled, and the set-up does not contain a load cell for force measurement as typical for a mini-tensile tester. To estimate the force, and therefore the strain, in the specimen, strain gauges are placed on one of the holders. During the experiment, the strain gauges will indicate the load level on the holder, which is the same as the load on the specimen. The value is given on the display of the strain gauge box.

A full strain gauge bridge (Wheatstone bridge) can either give an enhanced or a more precise signal than quarter- and half bridges. This is due to the fact that outputs from the four resistors add up if they are connected as can be seen in Figure 8 with the two transversal resistors on opposite sides of the circuit and likewise with the longitudinal ones. This set-up gives an enhanced signal. If, on the other hand, the two longitudinal and the transversal resistors are placed next to each other in the circuit, the output signal is an average of those from the four strain gauges, and a smaller - but more precise - signal is obtained. The Wheatstone bridge used has an overall gauge factor of 2.6 (1 for each of the longitudinal and 1/3 for each transversal).

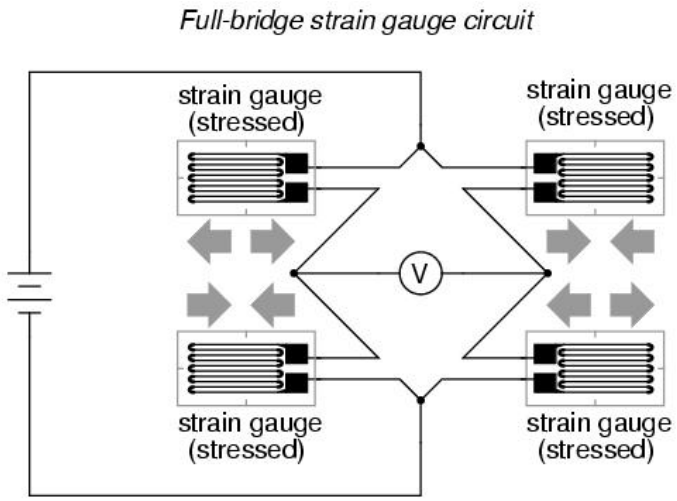

Figure 8: Full-bridge strain gauge circuit [7].

The connections on the holder are given as shown in Figure 9. The full bridge is used to get a signal as large as possible, since the strain of the holders is no more than about 0.01% for the current specimen and holder configuration. From the calibration data (see Section 4.5), the strain in the specimen can then be estimated. The method has the advantage that the output can be continuously monitored during the test via the display on the strain gauge box, and is quite accurate in the linear elastic region of the specimen. However, problems occur once the resin starts yielding as the force becomes nearly constant while the specimen undergoes large deformations. Consequently, the holder strain and gauge output will remain nearly constant from this point onwards.

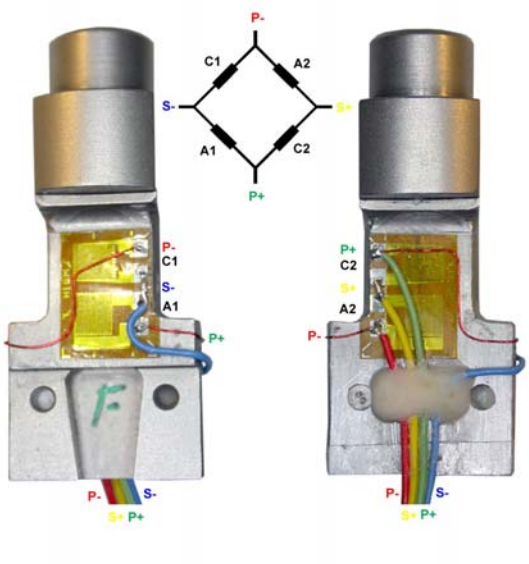

Figure 9: Front and back of specimen holder with strain gauges connected. In between a connection scheme for the Wheatstone bridge is shown. C1 and C2 are transverse resistors and A1 and A2 are longitudinal.

4.5 Calibration of Wheatstone bridge

The calibration is done on an Instron machine model 8532 with a ± 5kN load cell. The specimen holders can take a load of about 1kN. Stress-strain curve measurements of epoxy and polyester specimens were undertaken with an extensometer, while simultaneously measuring the strain in the holder with the strain gauge bridge. The output of the strain gauge box can then be used for strain level indication during the single fiber fragmentation test.

Such a typical calibration curve is shown in Figure 10. Up to 3% strain, the box output is found to give a good indication of the strain in the specimen. However, the problem of a constant strain output due to yielding of the specimen at higher strains is also clearly demonstrated for this type of material. Furthermore, the box output will also depend on the exact specimen geometry: the calibration curve is given for a polyester specimen with a cross-sectional area of 2 x 2 mm.

Approximate strain gauge box outputs at some strain levels are listed below. These values indicate the strain level in the specimens during the single fiber fragmentation test.

Epoxy specimens: 1 % ε = 40 με, 2 % ε = 95 με, 3 % ε = 130 με, 4 % ε = 140 με
Polyester specimens: 1 % ε = 30 με, 2 % ε = 80 με, 3 % ε = 115 με, 4 % ε = 125 με

The holder strains scale linearly with a different specimen area, and values can therefore be corrected. However, for a different type of material the calibration needs to be repeated.

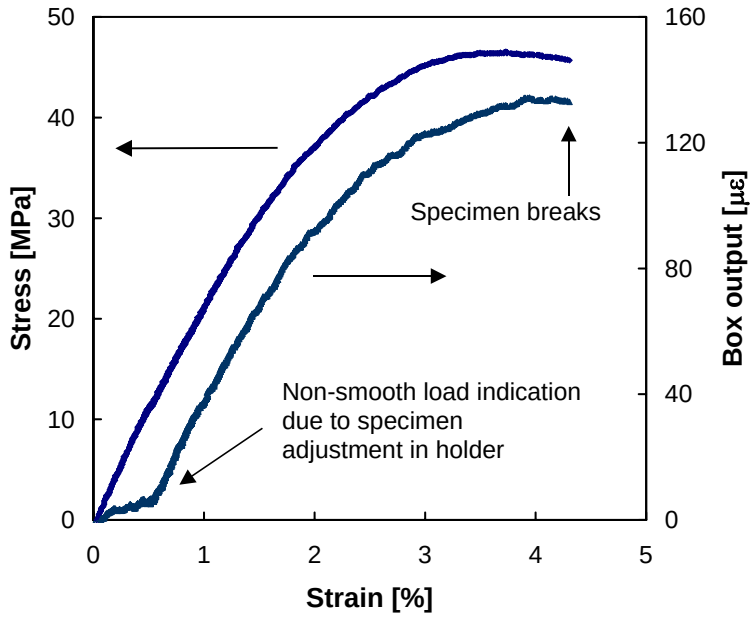

Figure 10: Holder calibration

4.6 Strain Measurement in Specimen

A more accurate measurement of the strain in the specimen is undertaken by placing markers on the specimen. These can consist of either two lines with permanent marker on the edge of the specimen or some small indentation marks made with a sharp tool. Care has to be taken to not damage the specimen, which will lead to early failure. For each strain level investigated, a picture is taken and the distance between the markers is measured afterwards. Markers should be placed at a distance of less than 9mm so that they can be saved on one digital picture with the 1.6 magnification objective. This technique has the following advantages over putting additional strain gauges on the specimen: (1) The method requires less preparation time, (2) the markers need considerably less space and (3) there is no limit for the maximum strain to be measured (strain gauges normally measure accurately up to 3% strain).

4.7 Pictures with cross-polarised light

Cross-polarised light can be used to see stress and strain patterns in the area around a fiber break. This phenomenon is called birefringence. Although birefringence is an inherent property of many anisotropic crystals, such as calcite and quartz, it can also arise from other factors, such as structural ordering, physical stress, deformation, flow through a restricted conduit, and strain. **Stress** and **strain** birefringence occur due to external forces and/or deformation acting on materials that are not naturally birefringent. Examples are stretched films and fibers, deformed glass and plastic lenses, and stressed polymer castings.

In the interface region, the binding pattern becomes disturbed when a crack occurs. A region of interfacial shear stresses and frictional stresses is created in the matrix, which appear coloured when cross-polarised light is transmitted through as explained in Figure 11. Apart from in the interface region, both fiber and matrix will appear dark as they are normally non-birefringent materials.

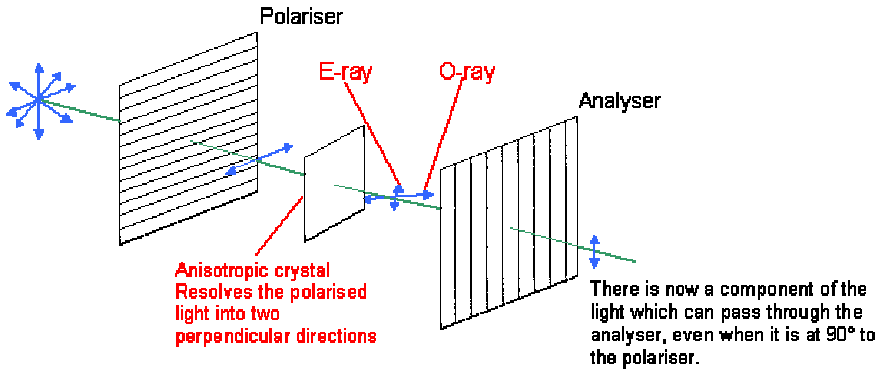

Figure 11: Cross-polarisation. Two polarizers with perpendicular polarisation direction with an anisotropic material in between [12].

5 Result Interpretation

The single fiber fragmentation test offers different possibilities for the interpretation of the interfacial adhesion between fiber and matrix. Data processing consists of the calculation of an interfacial adhesion parameter either from the distribution of fragments lengths using a force balance approach based on the Kelly-Tyson model [7], or from the measurement of debonding length using energy balance schemes [3]. Furthermore, an optical investigation of the crack shape around the area of fiber breaking also gives a good indication of differences in the adhesion of fiber and matrix. The following sections explain the standard data analysis methods, which are also of use for industrial testing purposes. The examples are taken from our own research with glass fibers and epoxy and polyester resins, as well as the literature.

5.1 S – Shape Behaviour

This type of analysis records the matrix strain and the according number of fiber breaks. For low strains, no fiber breaks will occur until the fiber failure strain is reached. After the first fiber break, the frequency will increase and slow down again while reaching saturation [3]. A plot of this S-shaped behaviour can be seen in Figure 12 for glass and carbon fibers in comparison. As carbon fibers are more brittle, their fragmentation process will start earlier.

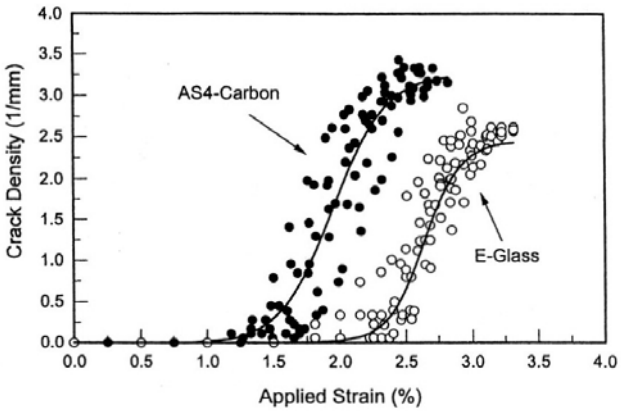

Figure 12: Crack density versus applied strain for E-Glass fibers and AS4-Carbon fibers [3].

Figure 13 shows the same behaviour for some of the tests undertaken at AFM-Risø for E-glass fibers with different surface treatments and polyester resin as matrix. A least squares fit with an exponential function was used for fitting the data points [3]. TMPP (trimethoxysilylpropyl modified polyethylenimine) and AHAT (N-(6-aminohexyl)aminopropyltrimethoxysilane) sized fiber exhibit a significantly larger amount of fiber breaks than the commercial sizings. The curves therefore clearly indicate a successful modification of the interface between fiber and matrix. For TMPP and AHAT sized fibers, the failure onset is about 2 to 2.5 % as also shown in Figure 12. This failure onset is reasonable as the failure strain of the tested E-glass fibers is 2±0.5% [11]. Compressive fiber strains introduced during manufacture will shift the specimen strain at fracture onset to slightly higher values.

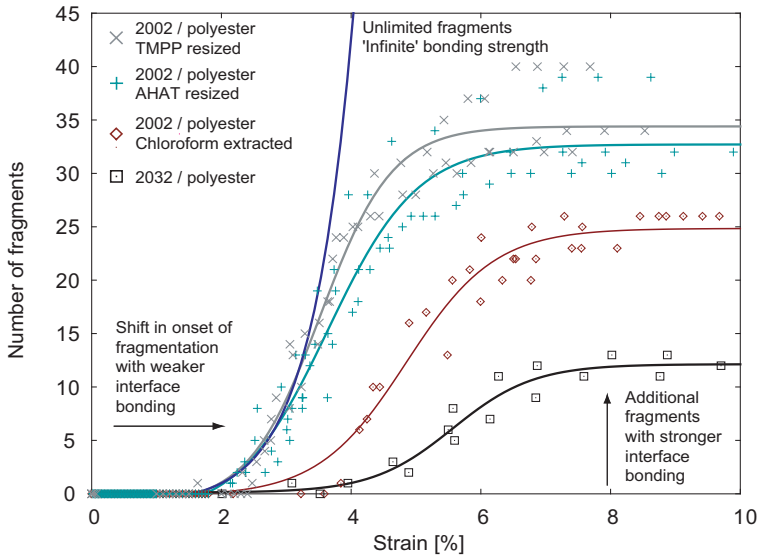

Figure 13: S-curves for different types of surface treatment.

For the same resin system and manufacturing procedure, the onset of fiber fragmentation should only depend on the fiber, but not on the surface treatment if (1) the fiber is bonded uniformly to the resin and (2) the surface treatment does not influence the fiber strength. Figure 13, however, clearly shows a shift to a *later* fragmentation onset with weaker interface bonding. It is postulated that this is might be due to partial fiber debonding prior to first fiber fracture, thereby resulting in a lower fiber strain and later fragmentation onset. Areas of debonding prior to fragmentation could be observed during the fragmentation test, but the mechanism of the fracture delay can currently not be explained. A reduction in fiber strength could also be used as an explanation for the shift in fragmentation onset. However, it has been shown in a related project investigating single fiber strength [11] that only small differences can be seen in the Weibull distribution for fiber strength (the sized fiber is stronger than the unsized fiber), which cannot explain a decrease in failure strain from 4% to 2%. Similarly, the re-sizing of fibers could also introduce damage to the fibers. This explanation is not considered in this context as the two commercially sized fibers also show considerable differences in debonding onset. The original 2002 / polyester is not shown in the plot above, but is similar to the chloroform extracted 2002 / polyester distribution. The 2032 / polyester in comparison shows a significantly delayed onset of fracture. The explanation of debonding prior to fragmentation is furthermore backed up by the observation that for a minimum threshold of interfacial shear strength (or number of fragments) the fracture onset strain remains constant (see TMPP and AHAT treatments). Based on these curves, a theoretical curve of infinite bonding strength can be included, which assumes repeated fragment splitting at the initial fragmentation rate of AHAT and TMPP treatments between 2 and 3% strain.

5.2 Fragmentation length

Upon saturation of the fragmentation, the individual fragment lengths are measured while keeping the specimen loaded. Figure 14 shows typical microscope pictures with a fragment length indicated between two fiber breaks. The interpretation of the crack shape is given in the next section.

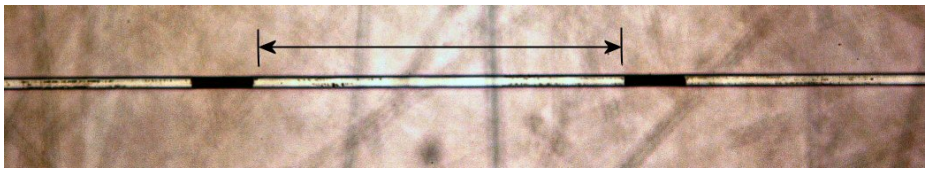

(a)

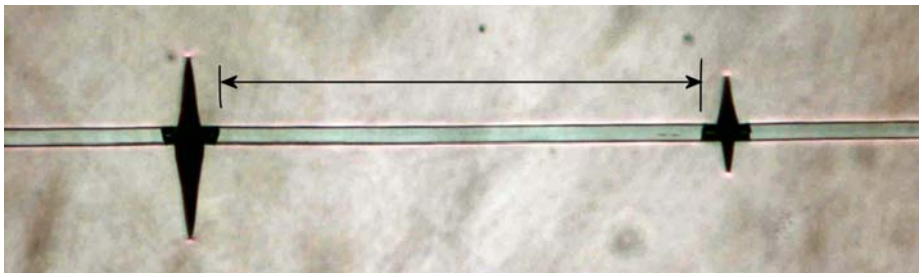

(b)

Figure 14: Part of fragmented fiber in polyester matrix. The black areas represent the cracks, the arrows indicate the fragment length. (a) As received, sized, glass fiber surface, (b) APTES modified surface.

A histogram plot as in Figure 15 can be used to visualise the distribution of fragment lengths. In this plot, the distribution of fragment lengths is shown as a histogram for the glass fiber/polyester specimens with different treatments. The fragment lengths vary between 100μm and 1700 μm. They are binned in intervals of 140 μm, where the value on the x-axis is the middle value of the interval. The histogram is a good way of comparing results of different distributions with respect to starting and end value, but also the distribution of fragments within the bins.

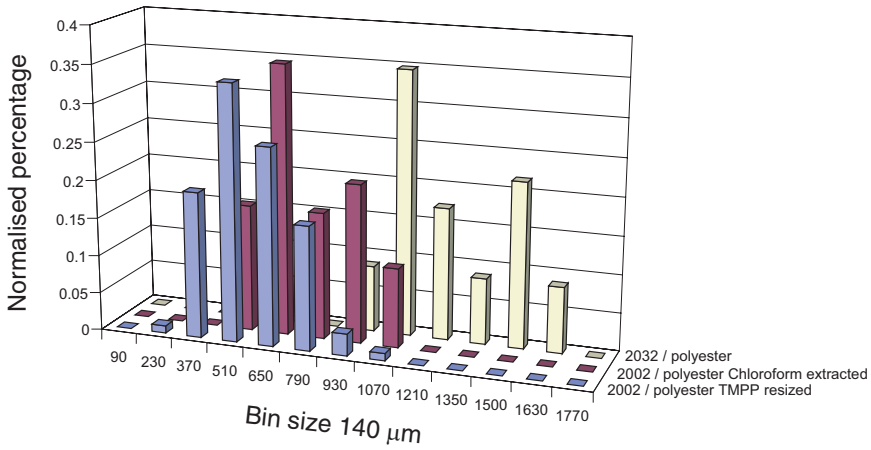

Figure 15: Histogram distribution of fragment lengths

The interfacial shear strength, τ, can be calculated with the following relationship [7]:

$$\tau = \frac{\sigma_f (l_c)\, d}{2 l_c},$$

where σ_f is the fiber strength at the critical length as evaluated from single fiber tests and Weibull statistics [11], d is the fiber diameter and l_c is the critical fragment length of the fiber. The critical fragment length is calculated from the average fragment length $\bar{l}$ by $l_c = 4/3\bar{l}$.

The fiber strength σ_f was experimentally obtained by Thraner [11], and needs to be corrected for the shorter critical fragment length by using Weibull statistics. This is explained in the Appendix.

Typical values for the above results are given in Table 2.

System	Critical fragment length [μm]	Fiber strength (adjusted) [MPa]	Interfacial shear strength [MPa]
2032 / polyester	1460	3045	18.5
2002 / polyester Chloroform extr.	807	3484	36.0
2002 / polyester TMPP resized	585	3750	53.8

Table 2: Shear strength calculation

5.3 Cumulative distribution of fragment length

Another way of plotting the information of fragment length distribution is the cumulative distribution [13] as shown in Figure 16. Here we are looking at two results: (1) The shift of the curve to higher or lower fragment lengths, which gives an indication of the adhesion between fiber and matrix, and (2) a change in shape of the cumulative plot, which can be due to the lower adhesion, but also due to differences in fiber strength variability.

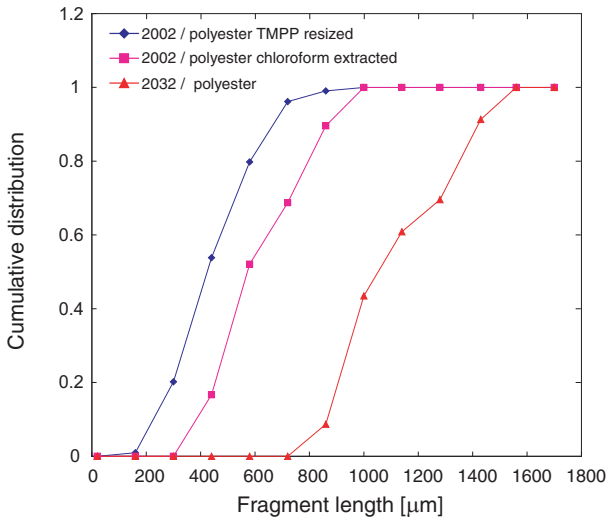

Figure 16: Cumulative distribution

5.4 Shape of breaks

The shape of the fiber breaks can give a significant indication of the strength of the bond between fiber and matrix. A strong bonding between fiber and matrix often introduces damage to the matrix in the area around the breaks, and the gaps between the fiber ends are of the order of the fiber diameter. With increasing stress, most of them expand but to not more than twice their initial gap length. The deformation into the resin often starts by forming a V-shape on one side of the fiber break and two smaller ones on the other side. For very strong interface bonding, extensive crack propagation into the matrix can occur and also lead to specimen failure [14].

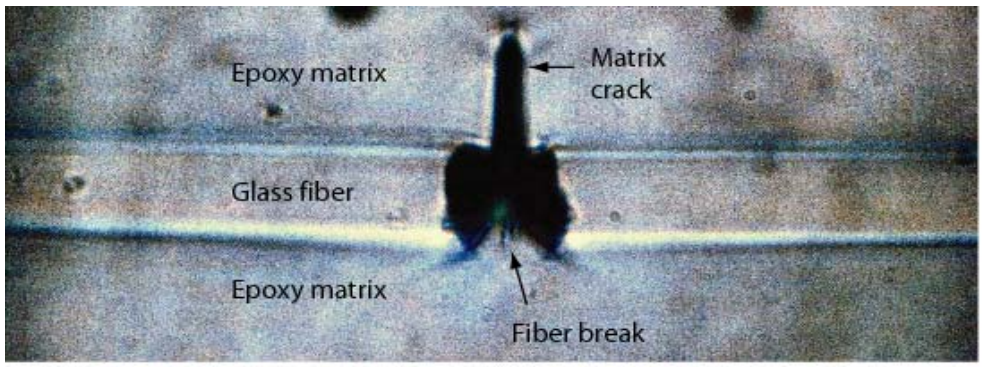

Figure 17: Strong bonding between fiber and matrix causes cracks to propagate into the matrix system.

For a weak interface system, on the other hand, most of the fiber cracks do not damage the resin and show immediate widening of the breaking gap. An example of this can be seen in Figure 18. Raman spectroscopy confirmed that the black area is indeed a hollow core apart from the middle where some fiber fragments can be detected [15]. Some of these gaps became more than 5 times wider than the fiber diameter with further loading.

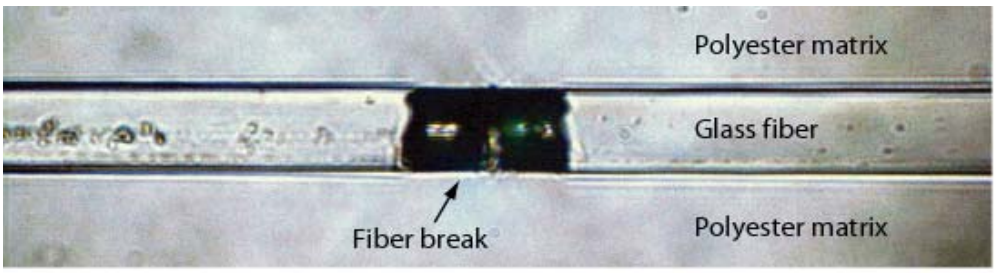

Figure 18: Weak bonding between fiber and matrix causes only very little damage in the matrix. The fiber has slipped, thereby widening the gap between the fiber ends considerably.

Previous tests on macroscopic properties [16] identified transverse strength values of 30 MPa (strong) and 14.5 MPa (weak) for the two systems, thereby justifying the interpretation of strong and weak interface bonding.

5.5 Photoelastic features

Using cross-polarised light, the region around the fiber breaks exhibits a coloured pattern. This is called the birefringence, or photoelastic pattern. The phenomenon in the case of single fiber composites is caused by the interfacial shear and frictional stresses and strains at the interface. It can be seen that these stresses occur symmetrically around a given fiber break. Upon saturation, the ends of these patterns almost touch each other (see Figure 19 (b) and (c)), thereby indicating that shear stress transfer takes place over the whole fragment length. Further fiber breakage is then unlikely.

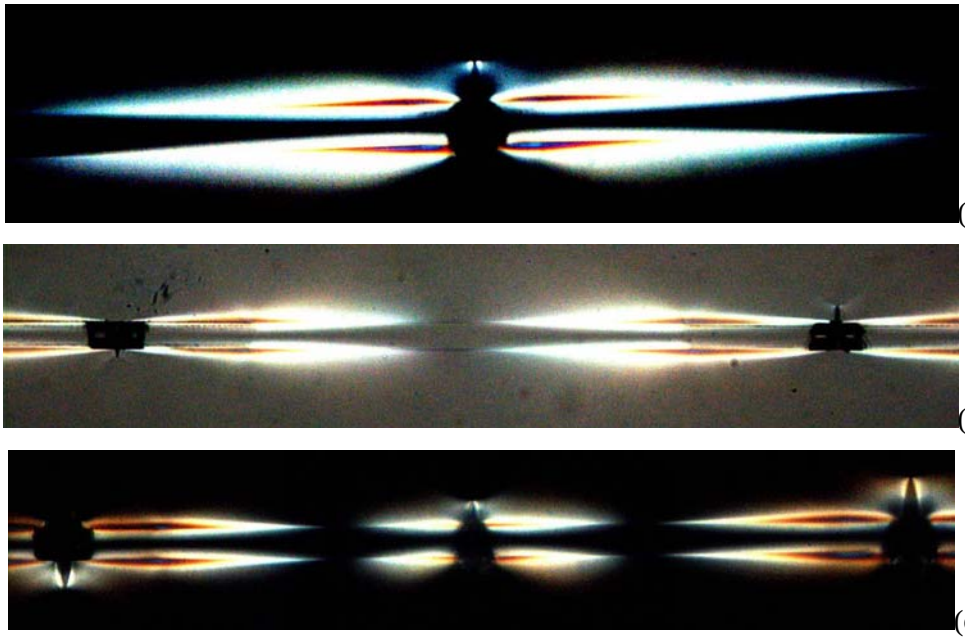

Figure 19: Interface patterns seen by using cross-polarized light for an epoxy resin. a) One crack with a deformation into the epoxy on the top around which the plane polarized light is also visible. b) Two neighbouring cracks. c)Three neighbouring cracks.

The birefringence method to determine fiber breaks is required when carbon fibers are used. As they are not transparent, it is not easy to find the fiber breaks if the cracks do not propagate into the surrounding matrix. In these cases, the photoelastic pattern can be investigated instead.

During our studies it has been found that epoxy systems exhibit very extensive birefringence, which can still be seen once the specimen is unloaded. For polyester matrix systems, on the other hand, the birefringence is less clear and also disappears very quickly once the specimen is unloaded.

5.6 Debonding Zone

For fiber-reinforced composites, one of the most important concerns is to observe interfacial debonding phenomena between fiber and polymeric matrices. When a fiber fractures in the fragmentation test, debonding between the fiber and the matrix often occurs simultaneously, depending on the strength of the bond. Thus, the observation of fiber fracture is also a tool for understanding the interfacial debonding process.

The birefringence patterns have been used in the literature [3] to determine the debonding length at each fiber break for epoxy resins. Theoretically, the highest shear stress in the fiber should be found near the end of the fragment (zero tensile stress). However, if a debonding process accompanies the fiber break, the shear stress will decrease to zero in the debonded region. Figure 20 compares the two expected birefringence patterns for fiber breaks without debonding and fiber breaks with debonding.

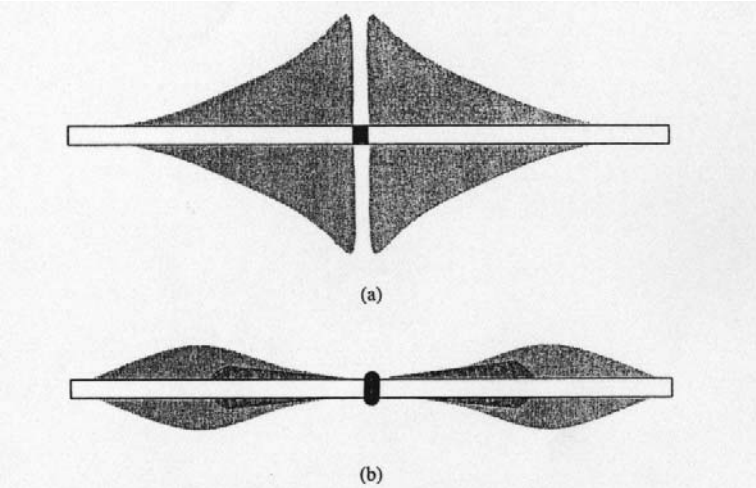

Figure 20: The schematic feature of photoelastic birefringence of shear stress around a fiber break. (a) Without debonding, (b) with debonding. After Kim and Nairn [3].

Comparing loading and unloading in the birefringence patterns, determination of the length of the debonded zone is shown in Figure 21. According to Kim and Nairn's [3] observations, the birefringence around the fiber break had two distinctly different colours; a red colour zone at the interface between fiber and matrix near the fiber break gap and a larger birefringence around the red zone. Upon unloading, the larger birefringence disappeared, but the inner red colour band was still visible. The authors assumed that, during loading, the length of the debond zone was therefore equal to the length of the red colour zone at the interface as indicated in the figure.

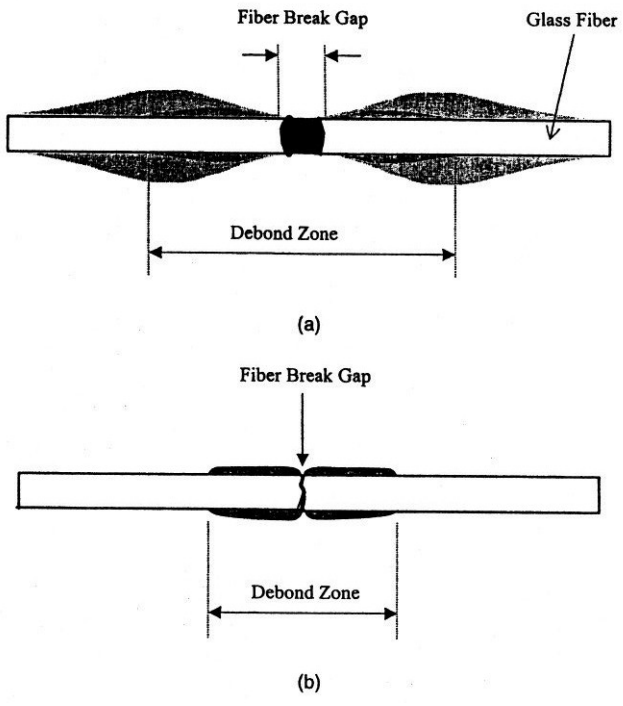

Figure 21: Schematic feature of debond zone of E-glass fiber. (a) Loading-applied state, (b) Loading-released state. After Kim and Nairn [3].

However, from our own observations, we think that the debonding zone should in fact be described differently. Figure 22 shows the comparison of the photoelastic birefringence pattern and the white light picture for a glass fiber/epoxy specimen around fiber fracture. The white light pictures clearly shows a change of the fiber surface on the right and left side. This is defined as the debonding length and corresponds in fact to the maximum of the red/blue birefringence pattern. The debonding length in this definition is about half the value established by Kim and Nairn [3]. Further fiber breaks are currently investigated to obtain more information about the debonding lengths, and compared to analytical models to calculate the debonding length.

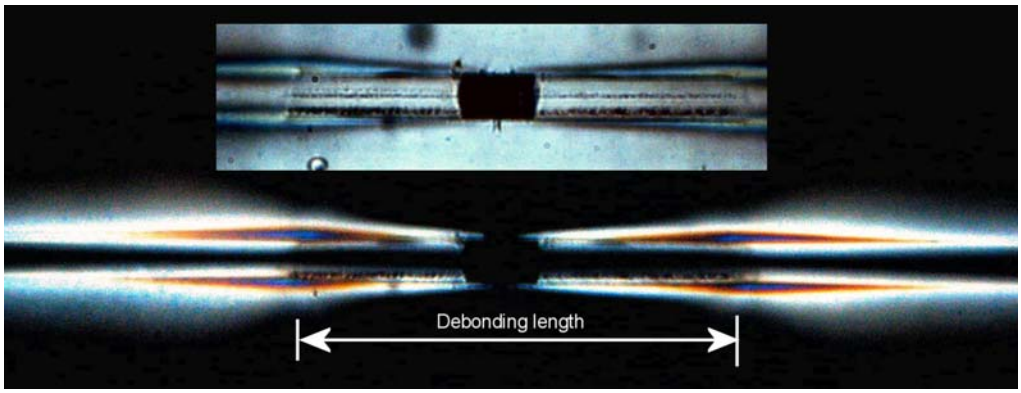

Figure 22: Debonding around gap in birefringence pattern and white light

After crack development, debonding between matrix and fiber can be observed with and without polarised light. Figure 23 shows this for the unloaded state. From

comparison of the two patterns, the debonding length is unclear in this case. Further investigations of the birefringence patterns are currently undertaken.

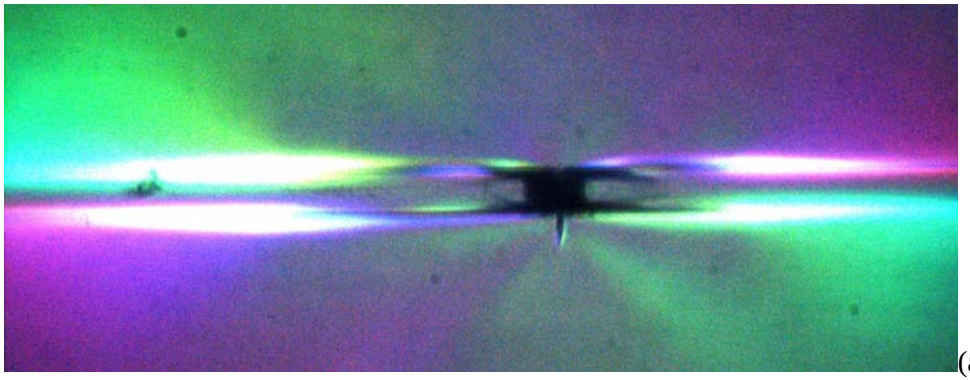
(a)

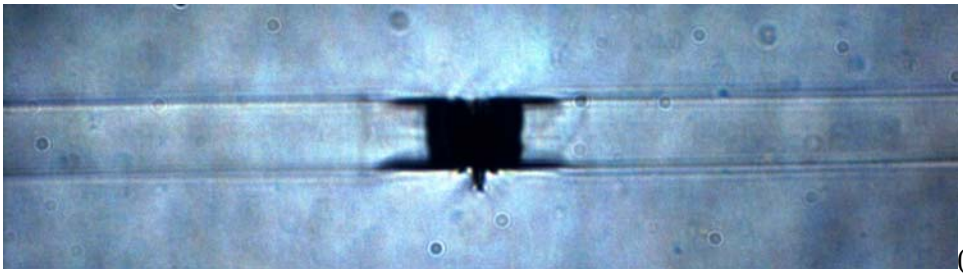
(b)

Figure 23: Debonding zones on cracks from epoxy specimens. The debonding zones are the black lines along the fiber with origin at the crack edges. a) Debonding zone lit by cross-polarized light during relaxation. b) Debonding zone lit by white light.

6 Summary

The test set-up and test procedure is described for the single fiber fragmentation test. As test results were found to vary in different laboratories, it is important to keep a fixed procedure for the test to guarantee repeatability of the results. Especially the specimen preparation is an important factor in this work. The report gives details about the pre-straining of the fibers and an estimation of the residual stresses present for typical resin systems.

The most important methods of result interpretation are described. They are by no means complete – the test offers advanced possibilities such as statistical data treatment with regard to Weibull statistics or advanced studies of the debonding behaviour during cracking, which can be related to energy balance methods for result interpretation. The research in this area regarding testing and modelling is on-going.

Appendix: Calculation of fiber strength at fragment length

A statistical analysis of the fiber tensile strength is commonly made by using the two-parameter Weibull distribution [11]. We can write the probability of failure $P_F(\sigma)$ of the fiber at a stress σ and length L as

$$P_F(\sigma, L) = 1 - \exp\left(-\frac{L}{L_0}\left(\frac{\sigma}{\sigma_0}\right)^m \right),$$

where m is the Weibull modulus, σ_0 the characteristic strength and L_0 is the gauge length. The Weibull modulus m is a measure of the scatter in the tensile data. The tests were undertaken for a fixed gauge length of 20mm. The values obtained for a typical glass fiber (diameter 16μm) were as follows:

σ_0 = 1680 MPa and
m = 4.4

This corresponds well to other values published in the literature [17]. For comparison of the characteristic strength value σ_0 at a different gauge length L_1, the above equation can be rewritten as

$$\sigma_0(L_1) = \sigma_0(L_0)\left(\frac{L_0}{L_1}\right)^{1/m} .$$

For the typical critical fragment length $l_c = L_1$=585 μm, this results in a characteristic strength of
σ_0 = 3750 MPa.

References

1. Pitkethly, M.J. et al. A round robin programme on interfacial test methods. Composites Science and Technology, 48, 205-214
2. Rich, M.J., Drzal, L. T., Hunston, D., Holmes, G. and McDonough, W. Round Robin Assessment Of The Single Fiber Fragmentation Test. Procedings of the American Society for Composites 17th Technical Conference, 2002.
3. Kim, B. W. and Nairn, J. A. Observations of Fiber Fracture and Interfacial Debonding Phenomena Using the Fragmentation Test in Single Fiber Composites. Journal of Composite Materials, 36, 1825-1858, 2002
4. Zhou, X.F., Nairn, J.A., Wagner, H.D. Fiber-matrix adhesion from the single fiber composite test: nucleation of interfacial debonding. Composites, Part A: 30, 1387-1400, 1999
5. Wagner, H.D. and Zhou, X.-F. A twin-fiber fragmentation experiment. Composites Part A, 29, 331-335, 1998
6. Feresenbet, E., Raghavan, D. and Holmes, G.A. The influence of silane coupling agent composition on the surface characterisation of fiber and on fiber- matrix interfacial shear strength. The Journal of Adhesion, 79, 643-665, 2003
7. Kelly, A. and Tyson, W.R. Tensile properties of fiber-reinforced metals: copper/tungsten and copper/molybdenum. Journal of the Mechanics and Physics of Solids, 13, 329-350, 1965
8. Ohsawa, T. Nakayama, A., Miwa, M. and Hasegawa, A. Temperature dependence of critical fiber length for glass fiber-reinforced thermosetting resins. Journal of Applied Polymer Science, 22, 3203-3212, 1978
9. Detassis, M, Pegoretti, A, Migliaresi, C and Wagner, HD, Experimental evaluation of residual stresses in single fibre composites by means of the fragmentation test, Journal of Materials Science, 31, 2385-2392, 1996
10. Wang, H.B., Yang, Y.G., Yu, H.H. and Sun, W.M., Assessment of residual stresses during cure and cooling of epoxy resins, Polymer Engineering and Science, 35(23), 1995
11. Thraner, A., Feih, S. and Lilholt, H. Establishing a Testing Procedure for Single-fiber Testing with Emphasis on Glass Fibers. Risø National Laboratory, Risø-I-2114(EN), 2003
12. http://www.cam.ac.uk/doitpoms/tlplib/CD1/pmicroscopy.php, Polarised light microscopy, University of Cambridge.
13. Zafeiropoulos, N.E., Baillie, C.A. and Hodgkinson, J.M. Engineering and characterisation of the interface in flax fibre/polypropylene composite materials. Part II. The effect of surface treatments on the interface. Composites Part A, 33, 1185-1190, 2002

14. Ho, A., Netravali, A.N. and Phoenix, S.L. Interfacial shear strength studies of Nicalon fibers in epoxy matrix using single fiber composite test. Polymer Composites, 16 (6), 542-548, 1995

15. Kislev, T., Marom, G., Berglund, L, Joffe, R., Nairn, J.A. and Wagner, H.D. On the nature of the opaque cylindrical regions formed at fiber break sites in a fragmentation test. Advanced composite letters, 11(1), 2002

16. Feih, S., Wei, J., Kingshott, P. and Lilholt, H. Interfacial Characterisation of Commercial Glass Fibers for Rotor Blades. 2. Mechanical Characterisation. Risø National Laboratory, Risø-I-1992(EN), 2003

17. Cheng, T.-H., Jones, F.R. and Wang, D. Effect of fiber conditioning on the interfacial shear strength of glass-fiber composites, Composites Science and Technology, 48, 89-96, 1993

Mission

To promote an innovative and environmentally sustainable technological development within the areas of energy, industrial technology and bioproduction through research, innovation and advisory services.

Vision

Risø's research **shall extend the boundaries** for the understanding of nature's processes and interactions right down to the molecular nanoscale.

The results obtained shall **set new trends** for the development of sustainable technologies within the fields of energy, industrial technology and biotechnology.

The efforts made **shall benefit** Danish society and lead to the development of new multi-billion industries.